IEEE Access
Multidisciplinary | Rapid Review | Open Access Journal

Received February 20, 2021, accepted February 27, 2021, date of publication March 2, 2021, date of current version March 17, 2021.

Digital Object Identifier 10.1109/ACCESS.2021.3063434

Optimal Control for Speed Governing System of On-Grid Adjustable-Speed Pumped Storage Unit Aimed at Transient Performance Improvement

WENXIA PAN[1,2], ZHU ZHU[1,3], TONGCHUI LIU[1,4], MINGYANG LIU[5], (Member, IEEE), AND WEI TIAN[1,6]

[1]College of Energy and Electrical Engineering, Hohai University, Nanjing 210098, China
[2]Research Center for Renewable Energy Generation Engineering, Ministry of Education, Hohai University, Nanjing 210098, China
[3]College of Electrical Engineering, Tongling University, Tongling 244000, China
[4]State Grid Ningbo Power Supply Company, Ningbo 315200, China
[5]State Grid Henan Electric Power Research Institute, Zhengzhou 450052, China
[6]NARI Technology Company Ltd., Nanjing 211000, China

Corresponding author: Zhu Zhu (zhuzhu515@hhu.edu.cn)

This work was supported in part by the National Natural Science Foundation of China under Grant 51377047, and in part by the 111 Project of Renewable Energy and Smart Grid under Grant B14022.

ABSTRACT Having great performance on active power regulation, grid-connected adjustable-speed pumped storage unit (ASPSU) has attracted world-wide concern. This superior transient response is achieved by both its excitation system and speed governing system, but dynamic characteristics study of ASPSU taking into account the optimal control of speed governor has seldom been explored. This paper first presents small-signal-stability model of on-grid ASPSU. Furthermore, instead of the dynamic-performance-indexes rule, a stability-degree criteria is proposed to optimize parameters for the speed regulator of ASPSU, which aims at improving the dynamic behavior of rotational speed and guide vane opening. Firstly, a mathematical model of on-grid ASPSU with power priority control is derived and it is validated by comparing simulated performance with on-site measurements of a Japanese commissioned ASPSU. Secondly, the small-signal-stability model is showcased, and the influence of control parameters on the stability degree which builds the bridge between eigenvalues and transient performance is investigated in details. Thirdly, instead of improved integral of time-weighted-absolute-error criteria, a novel stability-degree criteria is utilised in particle swarm optimization algorithm to optimise the regulator's parameters of ASPSU. Finally, with the optimised parameters, the indicial response of a 400MW on-grid ASPSU built with PSCAD/EMTDC is significantly enhanced.

INDEX TERMS Adjustable-speed pumped storage unit (ASPSU), speed governing system, stability degree, small-signal-stability model, particle swarm optimization (PSO) algorithm.

NOMENCLATURE

ω_m^*	command value of rotational speed
ω_m	real-time value of rotational speed
k_{p0}	proportional gain of governor
k_{i0}	integral gain of governor
T_a	equivalent time constant of pilot valve and servo motor
t_m	per unit deviation of mechanical torque
q	per unit deviation of flow
h	per unit deviation of head
ω	per unit deviation of rotational speed
y	per unit deviation of guide vane opening
e_h	partial derivative of mechanical torque with respect to head
e_ω	partial derivative of mechanical torque with respect to speed
e_y	partial derivative of mechanical torque with respect to wicket gate opening
e_{qh}	partial derivative of flow with respect to head
$e_{q\omega}$	partial derivative of flow with respect to speed

The associate editor coordinating the review of this manuscript and approving it for publication was Dwarkadas Pralhaddas Kothari.

e_{qy}	partial derivative of flow with respect to wicket gate opening
T_w	water time constant
T_J	inertia constant
T_m, T_{em}	mechanical torque and electromagnetic torque
T_{m0}	initial value of mechanical torque
R_s, R_r	resistances of stator and rotor
L_s, L_r	self-inductances of stator and rotor
L_m	mutual inductance
v_{sd}, v_{sq}	d, q-axis voltages of stator
v_{rd}, v_{rq}	d, q-axis voltages of rotor
i_{sd}, i_{sq}	d, q-axis currents of stator
i_{rd}, i_{rq}	d, q-axis currents of rotor
P_s^*	command value of active power on stator winding
P_s	real-time value of active power on stator winding
Q_s^*	command value of reactive power on stator winding
Q_s	real-time value of reactive power on stator winding
σ	leakage coefficient
ψ_{sd}, ψ_{sq}	d, q-axis magnetic fluxes of stator
p	pole number
s_r	slip frequency per unit
ψ_s	amplitude of magnetic flux of stator winding
V_s	amplitude of stator voltage
ω_s	synchronous rotational speed
k_{p1}	proportional gain of the power adjuster
k_{i1}	integral gain of the power adjuster
k_{p2}	proportional gain of the current adjuster
k_{i2}	integral gain of the current adjuster
V_b	voltage of the infinite bus
x_0, u_0, x_1	intermediate variables
x_2, x_3, x_4	intermediate variables

I. INTRODUCTION

Rocketing penetration of on-grid renewable energy sources into power system brings new challenges to active power balance. In modern power grid, conventional fixed-speed pumped storage unit plays an important role in active power regulation. Compared to the fixed-speed unit, adjustable-speed pumped storage unit (ASPSU) has greater potential in maintaining active power balance due to its variable rotational speed [1]–[3]. In order to fully explore this potential, it is vital and put into operation to optimize its transient performance on active power regulation.

ASPSU is mainly composed of AC excitation induction machine with its excitation system and reversible pump-turbine with its speed governing system, as illustrated in Figure 1. Previous studies on dynamic behavior of ASPSU have started from modeling and dynamic simulation [4]–[6]. Muljadi *et al.* detailed a hydrodynamic model and simulated by PSCAD/EMTDC [4]. Shi *et al.* established the ASPSU mathematical model and tested in RTDS simulation [5]. But both simulations are insufficient to compare results with the practical case. Belhadji *et al.* proposed a ASPSU model with permanent magnet machine and experimentally validated by a dedicated test rig [6]. Afterwards, to gain a better transient performance, some researches have focused on its excitation system, involving more suitable power converter topologies [7]–[9] and modified control schemes [10]–[12]. In terms of power converter itself, Bocquel *et al.* analyzed the benefits of a drive system which consists of a cyclo-converter driven supplied by ALSTOM and is installed in ASPSU of Goldisthal pumped storage power plant (PSPP) in Germany [7]. Wang *et al.* introduced the advantages of cascaded H-bridge multilevel converter, a type of back-to-back voltage source converter, which is adopted in Xiang Hong Dian PSPP in China [8]. Joseph *et al.* reviewed alternative power converter topologies (cycloconverter, back-to-back converter, matrix converter *et al.*) and modulation techniques (sinusoidal PWM, space-vector PWM, selective-harmonic-elimination PWM *et al.*) of excitation system in ASPSU [9]. With respect to the control development of excitation system, Lung *et al.* adopted PI controller with optimized parameters employed the cycloconverter of AC excitation induction machine and first obtained great dynamic characteristics similar to those of a 400MW practical example [10]. Ji *et al.* presented active disturbance rejection control instead of PI control for back-to-back converter of excitator and vertified the better dynamic performance by a 1.5MW ASPSU built with PSCAD/EMTDC [11]. Hu *et al.* provided a novel control method for back-to-back converter of excitation system which can provide faster reactive power support during fault periods [12].

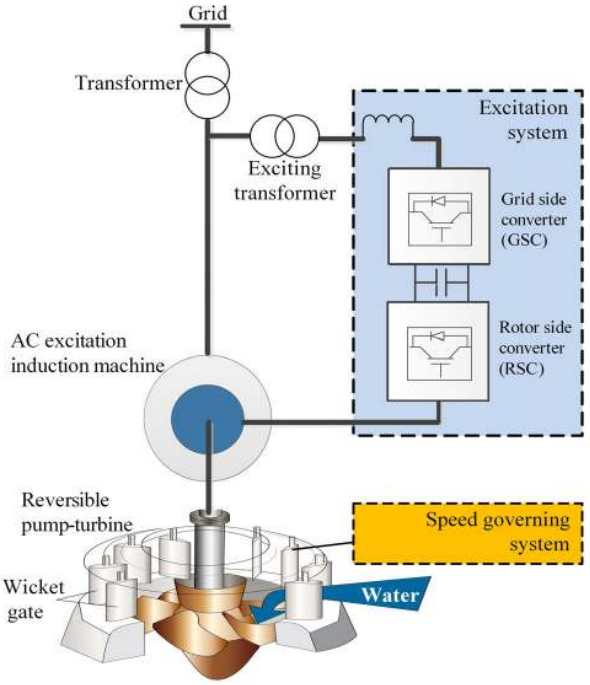

FIGURE 1. Typical structure diagram of ASPSU using back-to-back converters (figure modified from [4]).

However, the fact is that the great characteristics of ASPSU under load perturbation are realized by both its excitation system and speed regulation system [1], [13], [14]. It means that the preferable traient performance of active power, rotational speed and wicket gate opening of ASPSU depends on both excitator and speed governor. Therefore, power regulation characteristics of ASPSU can be promoted by not only the modification of excitation system but also the development of speed governing system, specially, optimization of speed adjustment control techniques.

Studies on optimal control for speed governor of on-grid ASPSU have seldom been reported. Basically, there are four rules for optimizing governor parameters of ASPSU, i.e. integral of square-error (ISE), integral of absolute-error (IAE), integral of time-weighted-squared-error (ITSE), and integral of time-weighted-absolute-error (ITAE) which is also the most widely used [15]. ITAE was proposed by Graham and Lathrop (1954), and can often provide controllers with a high load disturbance rejection and minimize the system overshoot [16]–[19]. Based on it, Xu *et al.* researched on parameters optimization by improved-ITAE criteria [20].

Nevertheless, these criterion all depend on external transient behavior indexes. Different from these indexes, the stability degree is a crucial factor in dynamic characteristics of ASPSU [21], and it is probable to develop a stability-degree criteria for optimizing control for speed governor of on-grid ASPSU. Motivated by discussions above, the current paper concentrates on speed governing system of on-grid ASPSU to develop its dynamic performance. Specifically, (1) first establishes small-signal-stability model of on-grid ASPSU, (2) on basis of this model, analyzes the influence of control parameters on the stability degree of ASPSU, (3) introduces a new stability-degree criteria for optimizing governor's parameters.

Apart from introduction, Section II derives the mathematical model of grid-connected ASPSU including its controllers, and then verifies the correctness of the model by comparing simulated behavior with that of a 400MW commissioned one. Section III deals with the small-signal-stability model and examined the effect of control parameters on the stability degree which builds the bridge between eigenvalues and transient performance. Section IV describes a novel optimal tuning method which uses a stability-degree criteria instead of improved-ITAE rule for governor of ASPSU in particle swarm optimization (PSO) algorithm. Section V performs the indicial response of a 400MW grid-connected ASPSU model with optimal control parameters in PSCAD/EMTDC simulation. The main contributions and conclusions are condensed in Section VI.

II. ASPSU MATHEMATICAL MODEL

ASPSU can have significant development in regulation time of power output under load disturbance, being able to utilize the flywheel effect from the rotating masses [22]. Hence, great dynamic performance of on-grid ASPSU is acquired by coordinated control between excitation system and speed governing system. Generally, there are three alternative coordinated control approaches [13], [14].

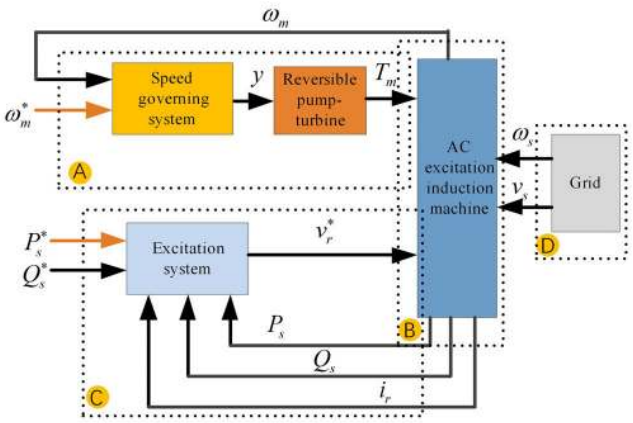

FIGURE 2. Brief block diagram of the integrated ASPSU using fast power control.

Strategy 1: The electrical power is controlled by converter, and the rotational speed is controlled by regulator adjusting the guide vane opening (Fast Power Control).

Strategy 2: The rotational speed is controlled by converter, and the electrical power is controlled by regulator adjusting guide vane opening (Fast Speed Control).

Strategy 3: A combination of the two approaches above.

Because the power converter can be tuned very quickly compared to gate opening, *Strategy 1* is labeled as Fast Power Control and *Strategy 2* is marked as Fast Speed Control. *Strategy 3* is implemented that Fast Speed Control is normally carried out while it is switched to Fast Power Control in the case of a large disturbance, which is adopted in Yagisawa and Shiobara plants in Japan [13], [14]. Fast Power Control is possibly considered as a better approach used in ASPSU regarding its transient behavior [1], [4], [13], [23]. Therefore, the combined control of ASPSU between excitation system and speed governing system is still being studied and Fast Power Control is employed in this work.

The brief block diagram of integrated ASPSU is described in Figure 2, including (A) speed governing system and reversible pump-turbine, (B) AC-excitation induction machine, (C) rotor side converter (RSC) control of excitation system, and (D) interfacing with power grid. Besides, the following variables without units are per unit values.

A. SPEED GOVERNING SYSTEM AND REVERSIBLE PUMP-TURBINE

At present, proportion-integration-differentiation (PID) controller is the most widely used in speed tuning system. However, Kundur concluded that the usage of a high deviative gain often results in excessive oscillations together with probable instability when the generating system is strongly connected to an interacted system [21]. Consequently, the derivative gain is usually set to zero, PI control now.

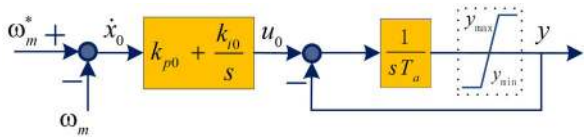

FIGURE 3. Block diagram of speed governing system.

To begin with, the block diagram of PI governor is shown in Figure 3. It describes the relationship between rotational speed error and guide vane opening. This relationship can be written as formula (1).

$$\begin{cases} \dot{x}_0 = \omega_m^* - \omega_m \\ u_0 = k_{p0}\dot{x}_0 + k_{i0}x_0 \\ u_0 = T_a\dot{y} + y \end{cases} \tag{1}$$

Here, ω_m^* and ω_m are command and real-time values of rotational speed respectively. x_0 and u_0 are the intermediate variables. k_{p0} and k_{i0} are proportional gain and integral gain respectively. T_a is the equivalent time constant of pilot valve and servo motor, with unit ''second''.

Next, the reversible pump-turbine is a complicated unit and its linearized model, based on the standard method with six coefficients for pump-turbine characteristics, is expressed as formula (2) [21], [24], [25].

$$\begin{cases} t_m = e_h h + e_\omega \omega + e_y y \\ q = e_{qh} h + e_{q\omega}\omega + e_{qy} y \end{cases} \tag{2}$$

Here, t_m, q, h, ω, and y are per unit deviations of mechanical torque, flow, head, rotational speed, and gate opening respectively. e_h, e_ω, and e_y are partial derivatives of mechanical torque with respect to head, rotational speed, and gate opening respectively. e_{qh}, $e_{q\omega}$, and e_{qy} are partial derivatives of flow with respect to head, rotational speed, and gate opening respectively. With typical values of coefficients, the relationship between per unit deviation of mechanical torque and vane opening can be given as formula (3) [10], [21]. Meanwhile, formula (3) and (4) are equivalent.

$$t_m(s) = \frac{1 - T_w s}{1 + 0.5T_w s} y(s) \tag{3}$$

$$t_m + 0.5T_w\dot{t}_m = y - T_w\dot{y} \tag{4}$$

The interface between A and B is commonly represented by a one-mass model shown by formula (5).

$$T_J\dot{\omega}_m = T_m - T_{em} \tag{5}$$

where, T_w is water time constant, with unit ''second''. T_J is inertia constant, with unit ''second''. T_m and T_{em} are mechanical torque and electromagnetic torque respectively. $T_m = T_{m0} + t_m$, and T_{m0} is initial value of mechanical torque.

B. AC-EXCITATION INDUCTION MACHINE

The state-space representation in the d-q reference frame is adopted for AC-excitation induction machine model, as described in equations (6)-(8), as shown at the bottom of the page [26], [27]. And currents including i_{ds}, i_{qs}, i_{dr}, and i_{qr} are shown as the state vector. Where, R_s and R_r are the resistances of the stator and rotor respectively. L_s and L_r are the self-inductances of the stator and rotor respectively. L_m is the mutual inductance. v_{sd}, v_{sq}, v_{rd}, and v_{rq} are the d, q-axis voltages of stator and rotor respectively. i_{sd}, i_{sq}, i_{rd}, and i_{rq} are the d, q-axis currents of stator and rotor respectively. σ is leakage coefficient.

The active power, reactive power, and electromagnetic torque on stator side are described in equation (9).

$$\begin{cases} P_s = \dfrac{3}{2}p\left(v_{ds}i_{ds} + v_{qs}i_{qs}\right) \\ Q_s = \dfrac{3}{2}p\left(v_{qs}i_{ds} - v_{ds}i_{qs}\right) \\ T_{em} = \dfrac{3L_m}{2L_s}p\left(\psi_{qs}i_{dr} - \psi_{ds}i_{qr}\right) = \dfrac{3}{2}pL_mI_m\left\{\vec{i}_s \cdot \vec{i}_r^*\right\} \end{cases} \tag{9}$$

Here, ψ_{sd} and ψ_{sq} are the d, q-axis magnetic fluxes of stator respectively. p is the pole number. P_s and Q_s are active power and reactive power on stator winding respectively.

When the stator flux direction is aligned with d-axis in the synchronous rotating d-q reference frame, q-axis component equals to zero. Thus, we have formula (10).

$$\begin{cases} \psi_{ds} = \psi_s = -V_s/\omega_s \\ \psi_{qs} = 0 \end{cases} \tag{10}$$

$$\begin{bmatrix} \dot{i}_{ds} \\ \dot{i}_{qs} \\ \dot{i}_{dr} \\ \dot{i}_{qr} \end{bmatrix} = \left(\frac{1}{\sigma L_s L_r}\right) A_0 \begin{bmatrix} i_{ds} \\ i_{qs} \\ i_{dr} \\ i_{qr} \end{bmatrix} + \left(\frac{1}{\sigma L_s L_r}\right) \begin{pmatrix} L_r & 0 & -L_m & 0 \\ 0 & L_r & 0 & -L_m \\ -L_m & 0 & L_s & 0 \\ 0 & -L_m & 0 & L_s \end{pmatrix} \begin{bmatrix} v_{ds} \\ v_{qs} \\ v_{dr} \\ v_{qr} \end{bmatrix} \tag{6}$$

$$A_0 = \begin{pmatrix} -R_s L_r & \omega_m L_m^2 + \omega_s \sigma L_s L_r & R_r L_m & \omega_m L_m L_r \\ -\omega_m L_m^2 - \omega_s \sigma L_s L_r & -R_s L_r & -\omega_m L_m L_r & R_r L_m \\ R_s L_m & -\omega_m L_m L_s & -R_r L_s & -\omega_m L_s L_r + \omega_s \sigma L_s L_r \\ \omega_m L_m L_s & R_s L_m & \omega_m L_s L_r - \omega_s \sigma L_s L_r & -R_r L_s \end{pmatrix} \tag{7}$$

$$\sigma = 1 - L_m^2 \Big/ L_s L_r \tag{8}$$

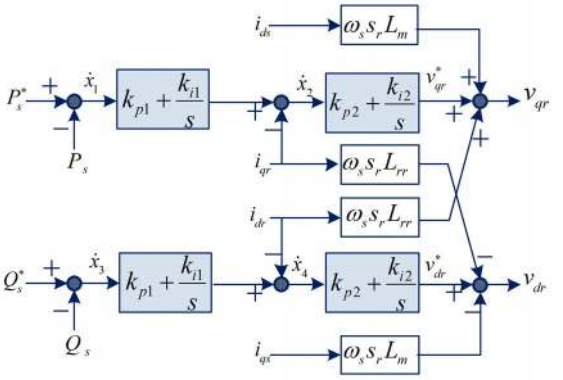

FIGURE 4. Block diagram of RSC control.

When $p = 1$, we have formula (11) by substituting (10) into (9).

$$\begin{cases} P_s = -\dfrac{3L_m}{2L_s} V_s i_{qr} \\ Q_s = \dfrac{3V_s^2}{2\omega_s L_s} - \dfrac{3V_s L_m}{2L_s} i_{dr} \\ T_{em} = \dfrac{3}{2} L_m \left(i_{qs} i_{dr} - i_{ds} i_{qr}\right) = -\dfrac{3L_m}{2L_s \omega_s} V_s i_{qr} \end{cases} \tag{11}$$

Here, ψ_s is amplitude of magnetic flux of stator winding. V_s is amplitude of stator voltage. ω_s is synchronous rotational speed.

C. RSC CONTROL

There are grid side converter (GSC) control and rotor side converter (RSC) control in the excitation system. Yet the active power regulation of AC-excitation induction machine is mainly controlled by RSC control, so RSC control model is presented as follows. Its block diagram is demonstrated in Figure 4 [28], and control equation is given by (12).

$$\begin{cases} \dot{x}_1 = P_s^* - P_s \\ \dot{x}_2 = k_{p1}\left(P_s^* - P_s\right) + k_{i1} x_1 - i_{qr} \\ \dot{x}_3 = Q_s^* - Q_s \\ \dot{x}_4 = k_{p1}\left(Q_s^* - Q_s\right) + k_{i1} x_3 - i_{dr} \\ v_{qr} = k_{p2}\left(k_{p1}(P_s^* - P_s) + k_{i1} x_1 - i_{qr}\right) \\ \qquad\qquad + k_{i2} x_2 + \omega_s s_r L_m i_{ds} + \omega_s s_r L_{rr} i_{dr} \\ v_{dr} = k_{p2}\left(k_{p1}\left(Q_s^* - Q_s\right) + k_{i1} x_3 - i_{dr}\right) \\ \qquad\qquad + k_{i2} x_4 - \omega_s s_r L_m i_{qs} - \omega_s s_r L_{rr} i_{qr} \end{cases} \tag{12}$$

where, k_{p1} and k_{i1} are the proportional and integral gains of the power adjuster respectively. k_{p2} and k_{i2} are the proportional and integral gains of rotor-side converter current adjuster respectively. P_s^* and P_s are command and real-time values of active power on the stator side respectively. Q_s^* and Q_s are command and real-time values of reactive power on the stator side respectively. x_1, x_2, x_3, and x_4 are the intermediate variables. s_r is slip frequency per unit and $s_r = 1 - \omega_m/\omega_s$. Besides $L_{rr} = L_r + L_m$.

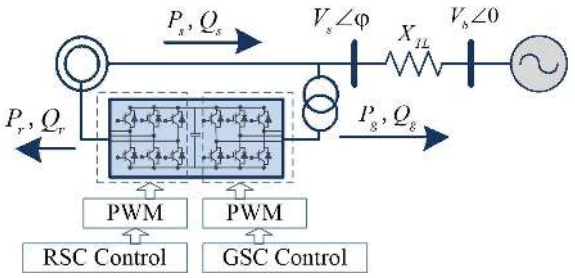

FIGURE 5. The interfacing with power grid.

D. INTERFACING WITH POWER GRID

The interfacing with power grid can be appeared in Figure 5, and written by equation (13) [6], [12], [29], [30].

$$\begin{cases} P_g = \dfrac{V_s V_b \sin\varphi}{X_{TL}} \\ Q_g = \dfrac{V_s^2 - V_s V_b \cos\varphi}{X_{TL}} \end{cases} \tag{13}$$

Here, V_b is the voltage of the infinite bus. X_{TL} is the combined reactance of the transformer and transmission line. $V_s\angle\varphi$ is the terminal voltage of stator side. P_g and Q_g are active and reactive power of grid respectively.

It is worth noting that the detailed description of the converters can be ignored. Since it is significant to model the transistors with very high frequency switching for research on fault process or high oscillations, while it is neglected to model the transistors for study on slow transient process like load perturbation in this work [26]. Moreover, because the eigenvalues associated with both GSC controller are far from the imaginary axis, the dynamics of the GSC controller can also be ignored [31].

E. ASPSU MODEL VALIDATION

This section is to verify the correctness of on-grid ASPSU model by comparing the transient behavior of time-domain simulation by PSCAD/EMTDC with on-site measurements in generating mode. The rated specifications of the 400MW ASPSU in Ohkawachi power station No. 4 are shown in Appendix A [1], [10], and model parameters used in simulation are given in Appendix B [26]. In addition, the tunable operations are described as follows [1], [10].

Grid-connected ASPSU operates in steady-state during 180s. The power command signal is increased by 0.1pu at t = 40s, and is decreased by 0.1pu at t = 94s. Starting at t = 40s, power output fast responds within 0.2s. Simultaneously, rotational speed and vane opening dynamically react within about 24s. Starting at t = 94s, power output also fast responds during 0.2s. Meanwhile, rotational speed and vane opening dynamically react during roughly 25s.

Significantly, on-site measurements are shown in nominal values in [1] as well as in per unit values in [10]. With reference to [10], per unit values are employed in comparisons in this work.

The comparisons in per unit values are demonstrated in Figure 6. There are four diagrams of dynamic

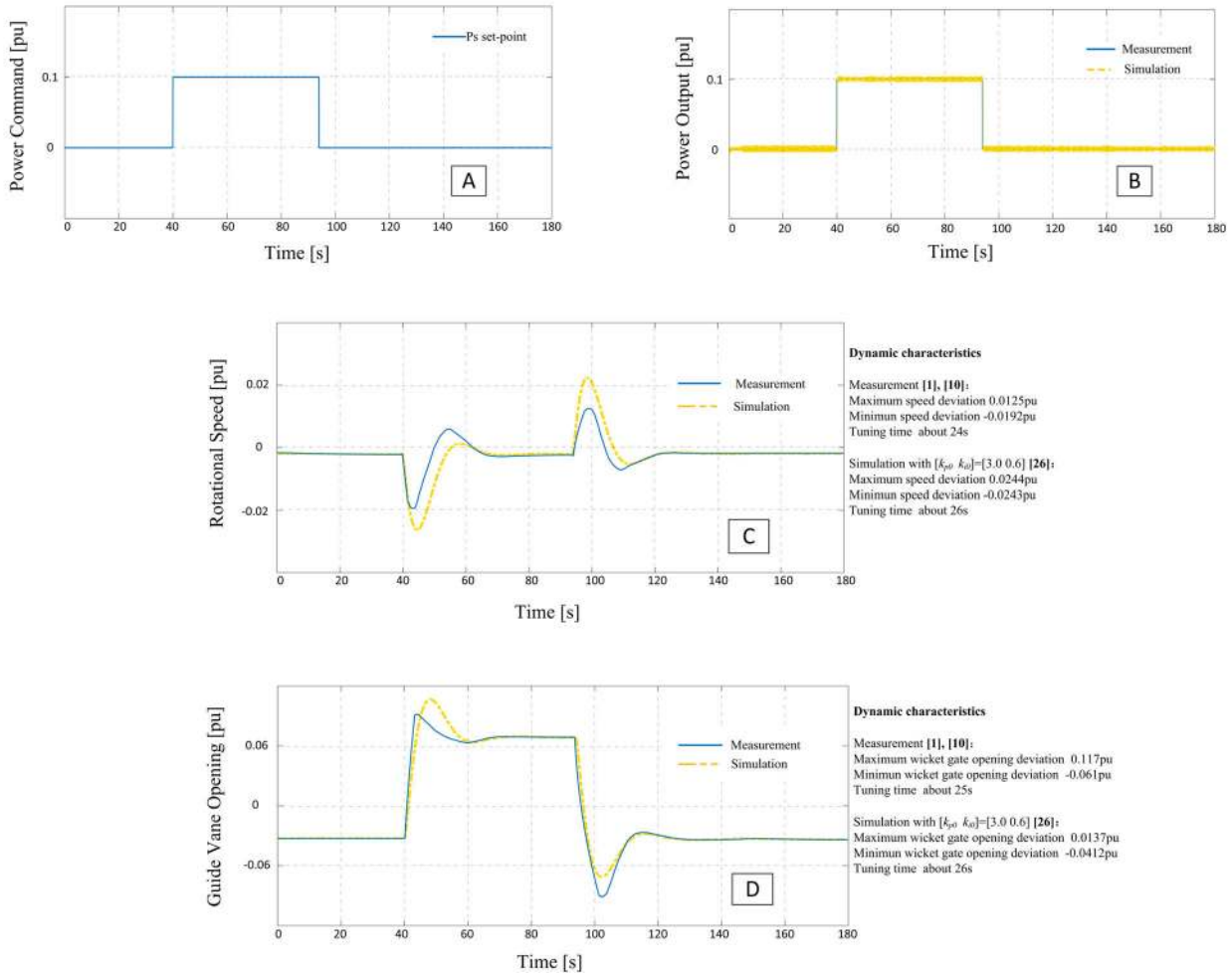

FIGURE 6. Comparisons of simulation and on-site measurements for ASPSU: (A) power command, (B) power output, (C) rotational speed, (D) guide vane opening.

characteristics, i.e. power command, power output, rotational speed, and guide vane opening. With the same power signal, measurements are revealed by the solid blue outlines, while simulations are plotted by the dashed yellow outlines.

According to comparisons showcased in Figure 6, it can be indicated that:

1) Fast response of power output is obtained with increased/decreased power command by means of rapid release/absorption of rotor kinetic energy because guide vane movement is insufficient to meet momentary power variations [13], [14];

2) Due to Fast Power Control employed in this work, tuning time of speed and wicket gate opening is nearly the same. But the regulation time is much longer than that of power output;

3) As for maximum and minimum deviations of speed and wicket gate opening, the simulation results are obviously worse than those of practice. It is very likely that governor control parameters are acquired not by optimization but simply from [26];

4) The slope of initial response of wicket gate is not as steep as that of the actual case. It is possible that the plant operating in practice adopts a direct control method of vane opening [10].

In summary, since characteristics (active power, rotational speed, and guide vane opening) have been correctly considered in anticipated model, the simulation achieves an agreement with the on-site measurements to validate the on-grid ASPSU model. Moreover, inadequate performances of runner speed and guide vane opening, resulting from casual control parameters setting, need to be improved.

III. SMALL-SIGNAL-STABILITY MODEL AND INFLUENCE OF CONTROL PARAMETERS ON STABILITY DEGREE

A. SMALL-SIGNAL-STABILITY MODEL

To sum up, equations (1), (4)-(8), (11)-(13) form the on-grid ASPSU dynamic model. And it can be shown in the compact form

$$\begin{cases} \dot{x} = f(x, z, u) \\ 0 = g(x, z, u) \end{cases} \tag{14}$$

where, x, z and u are the vectors of ASPSU state variables, control output variables, and input variables respectively. And they are given by

$$x = \left[x_0, y, t_m, \omega_m, x_1, x_2, x_3, x_4, i_{ds}, i_{qs}, i_{dr}, i_{qr}\right]^T,$$
$$z = \left[v_{dr}, v_{qr}\right]^T,$$
$$u = \left[\omega_m^*, P_s^*, Q_s^*, V_s, \omega_s\right]^T.$$

Linearing equation (14) at an operating point (x_0, z_0, u_0) when $u_0 = [1.038, 0.9, 0.0, 1.0, 1.0]$, small-signal-stability model of ASPSU can be obtained as formula (15).

$$\Delta\dot{x} = A_{sys}\Delta x \tag{15}$$

where, A_{sys} is the system state matrix, whose dimension is 12×12. And it is given by equation (16) [28], [32], [33].

$$A_{\text{sys}} = \left[A - BD^{-1}C\right]_{(\text{x}_0,\text{z}_0,\text{u}_0)} \tag{16}$$

where,

$$A = \begin{bmatrix} \frac{\partial f_1}{\partial x_1} & \cdots & \frac{\partial f_1}{\partial x_n} \\ \cdots & & \cdots \\ \frac{\partial f_n}{\partial x_1} & \cdots & \frac{\partial f_n}{\partial x_n} \end{bmatrix}; \quad B = \begin{bmatrix} \frac{\partial f_1}{\partial z_1} & \cdots & \frac{\partial f_1}{\partial z_m} \\ \cdots & & \cdots \\ \frac{\partial f_n}{\partial z_1} & \cdots & \frac{\partial f_n}{\partial z_m} \end{bmatrix};$$
$$C = \begin{bmatrix} \frac{\partial g_1}{\partial x_1} & \cdots & \frac{\partial g_1}{\partial x_n} \\ \cdots & & \cdots \\ \frac{\partial g_m}{\partial x_1} & \cdots & \frac{\partial g_m}{\partial x_n} \end{bmatrix}; \quad D = \begin{bmatrix} \frac{\partial g_1}{\partial z_1} & \cdots & \frac{\partial g_1}{\partial z_m} \\ \cdots & & \cdots \\ \frac{\partial g_m}{\partial z_1} & \cdots & \frac{\partial g_m}{\partial z_m} \end{bmatrix}. \tag{17}$$

Here, $n =$ the column number of the matrix and $n = 12$ in this work. $m =$ the row number of the matrix and $m = 2$ in this work.

Next, the eigenvalues λ_i of state matrix A_{sys} are solved as higher-order nonlinear expressions with excitator and governor parameters k_{p0}, k_{i0}, k_{p1}, k_{i1}, k_{p2} and k_{i2}. In order to guarantee system stable first, certain and appropriate excitation control parameters are carefully selected [34]. Then the eigenvalues λ_i with speed regulation control parameters are revealed by equation (18) and Table 1. The real components of the eigenvalues σ_i give the damping properties while the imaginary components of the eigenvalues ω_i give the oscillation characteristics. From Table 1, it can be seen that four of twelve eigenvalues are higher-order nonlinear functions of speed governing parameters k_{p0} and k_{i0}, the other eight eigenvalues which all have negative real parts are solved.

$$\lambda_i = \sigma_i \pm j\omega_i \quad (i \in 1, 2, \cdots, 12) \quad (\omega_i = 2\pi f_i) \tag{18}$$

In accordance with Lyapunov's first method that the stability in the small of a nonlinear system is determined by the eigenvalues of A_{sys}. When the eigenvalues have negative real parts, the original system is asymptotically stable. Whereas when at least one of the eigenvalues has a positive real part, the original system is unstable [21]. Hence, the real parts of eigenvalues must be negative in order to ensure the ASPSU system is stable. It means that the maximum real component of ones must be negative, as shown in formula (19).

$$\begin{aligned} &\text{Real}\,(\lambda_i) < 0 \quad (i \in 1, 2, \cdots, 12) \\ &i.e.\ \max\,(\sigma_i) < 0 \quad (i \in 1, 2, \cdots, 12) \end{aligned} \tag{19}$$

TABLE 1. The eigenvalues of state matrix A_{sys}.

No.	λ_i	No.	λ_i
		5,6	-1867±0.04i
		7,8	-0.67±58.39i
1	*higher-order*	9	-2.07
2	*nonlinear*		
3	*expressions with*	10	-25.28
4	k_{p0} *and* k_{i0}	11	-2.08
		12	-3.16

B. INFLUENCE OF CONTROL PARAMETERS ON STABILITY DEGREE

However, satisfying above stability constraint alone, with all eigenvalues in the left hand of S-plane, is not enough. Because in engineering application, it is common to shift the operation point or drift control parameters of speed regulator. As a result, the stability of ASPSU system can only be guaranteed if the stability degree improvement is as much as possible.

it must be emphasized that the stability degree is strong related to transient performance of system [21]. So it is convenient to enhance transient behavior of rotational speed and guide vane opening for ASPSU by improving stability degree of ASPSU system as much as possible. Usually, we can adopt eigenvalues in time-domain analysis to measure the stability degree, and we can also utilise gain-and-phase margin in frequency-domain analysis [32], [33], [35], [36].

In time-domain analysis, in order to optimize the stability degree of system, it can be used by developing its oscillation characteristics [33] or improving its decay properties [32], [35]. In ASPSU, oscillation frequencies f_i of electromagnetic state quantities is approximately 10Hz while those of electromechanical state quantities is around 0.1Hz [13], [14]. From this perspective, developing oscillation characteristics of ASPSU is dominated by electromagnetic state quantities. So optimizing decay properties by speed governor parameters is applied in the present paper.

Concretely, it can be accomplished to maximize the displacement of the nearest roots in front of the imaginary axis of the localization domain in S-plan, i.e. $|\max\,(\sigma_i)|$. And it has advantage of reducing the duration of the transient response and guarantee high stability degree of the system, which leads to the satisfactory performance of the control system [37].

Furthermore, within the typical ranges of k_{p0} and k_{i0}, $k_{p0} \in [0.5, 20]$ and $k_{i0} \in [0.05, 10]$ [20], [25], Figure 7 is drawn to visually present the influence of PI parameters on $\max\,(\sigma_i)$ of state matrix A_{sys} for ASPSU with MATLAB/SIMULINK.

The observation from Figure 7 shows that an index to measure the stability degree, $\max\,(\sigma_i)$, can be optimized at preferable speed governing parameters of ASPSU at suitable $[k_{p0}, k_{i0}]$.

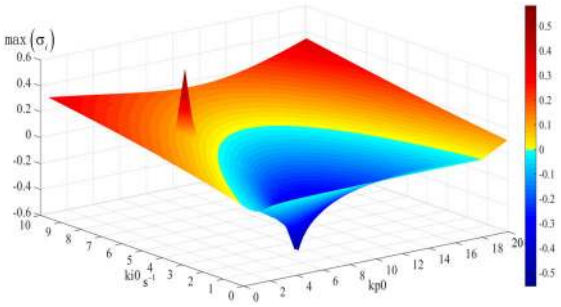

FIGURE 7. Influence of PI parameters on max (σ_i).

IV. PSO-BASED OPTIMAL CONTROL FOR SPEED GOVERNING SYSTEM OF ASPSU

PSO algorithm is employed to search the optimal parameters for the speed governing system of ASPSU in order to achieve the optimal transient performance.

A. BRIEF INTRODUCTION OF PSO ALGORITHM [38]–[40]

PSO, widely used in parameter optimization of governing systems of pumped storage unit [41]–[44]. Similar to other evolutionary computation techniques, the optimal solution is found through cooperation and competition among particles in a group in PSO algorithm. In details, the searching procedure for PSO is mainly divided into four steps. They are initialization, evaluation, updating, and stopping decision.

Step 1: it is to generate a group of particles where each one is a potential solution of the problem.

Step 2: it is to calculate the fitness value of each individual.

Step 3: each operator is updated velocity and position itself according to the fitness value to search other possible area.

Step 4: if the stopping criteria is satisfied, then stop, else go to *Step 2*.

In *Setp 3*, it includes velocity and position updating of particles. These velocity and position updating criterion are determined by formula (20).

$$\begin{cases} v_{i,j}(t+1) = w^{(t)} * v_{i,j}(t) + c_1 * rand() * \left(x^*_{i,j} - x_{i,j}(t)\right) \\ \qquad\qquad + c_2 * rand() * \left(x^*_j - x_{i,j}(t)\right) \\ x_{i,j}(t+1) = x_{i,j}(t) + v_{i,j}(t+1) \end{cases} \tag{20}$$

where, $i = 1, 2, \cdots, n$ as well as $j = 1, 2, \cdots, m$. Besides, n is the number of particles in a group, and each particle is a m-dimensional vector. $v_{i,j}(t)$ and $v_{i,j}(t+1)$ are the velocities of particle i in dimension j at time t and $t+1$ respectively. $w^{(t)}$ is inertia weight. c_1 and c_2 are the accelerating constants. *rand*() is a random number between 0 and 1. $x_{i,j}(t)$ and $x_{i,j}(t+1)$ are the positions of particle i in dimension j at time t and $t+1$ respectively. $x^*_{i,j}$, called pbest, is the best position which particle i has obtained so far. x^*_j, called gbest, is the best position which has been obtained by any particle among the group. And gbest is the candidate solution to the problem.

B. FITNESS FUNCTIONS UNDER DIFFERENT CONTROL SCHEMES

Traditionally, ITAE criteria is the most widely used to optimize parameters for speed governor of ASPSU [15]–[19]. When following the conventional method, the fitness function is shown as formula (21)-(22).

Minimize

$$J_{ITAE} = \int_0^{t_s} t\,|e(t)|dt \tag{21}$$

Bound

$$X_L \le X \le X_U \tag{22}$$

Nevertheless, ITAE criteria has been upgraded to minimize the overshoot and error calculation of system, as formula (23)-(24), called improved-ITAE criteria [20].

Minimize

$$J_{improved-ITAE} = \int_0^{t_s} [w_1 t\,|e(t)| + w_2 \delta(t)]dt \tag{23}$$

Bound

$$X_L \le X \le X_U \tag{24}$$

Here, t_s is tuning time. $e(t)$ is rotational speed error. $\delta(t)$ is output overshoot. w_1 and w_2 are weight coefficients. X is the solution vector. X_L and X_U are the lower limit and the upper limit respectively.

In current work, instead of improved-ITAE rule, a stability-degree criteria is utilised in PSO algorithm to optimise the regulator's parameters of ASPSU. And the objective function is illustrated by formula (25)-(26).

Minimize

$$J_{\text{stability degree}} = \max(\sigma_i) \tag{25}$$

Bound

$$\begin{aligned} X_L \le X \le X_U \\ \max(\sigma_i) < 0 \end{aligned} \tag{26}$$

In order to state the optimization process clearly, the flowchart of PSO as discussed is illustrated in Figure 8.

C. PARAMETER SETTINGS AND PSO SOLUTIONS

Firstly, to carry out fair comparison in fitness evaluation, population size of PSO algorithm with improved-ITAE rule and stability-degree criteria are both $N = 40$. The maximum generation is set to $G_k = 300$. The accelerating constants $c_1 = c_2 = 2$.

Secondly, it is considered that $w^{(t)}$ is critical to realize the global optimization ability of PSO algorithm, so a time varying $w^{(t)}$ linearly with decreasing weight strategy is utilized as formula (27) [39].

$$w^{(t)} = (w_{ini} - w_{end}) * \frac{(G_k - t)}{G_k} + w_{end} \tag{27}$$

where, the initial value of inertia weight $w_{ini} = 0.9$. The end value of inertia weight $w_{end} = 0.4$.

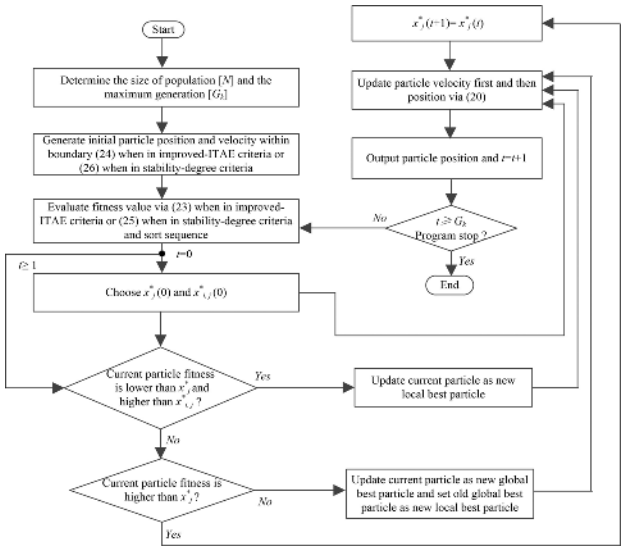

FIGURE 8. Flowchart of PSO scheme.

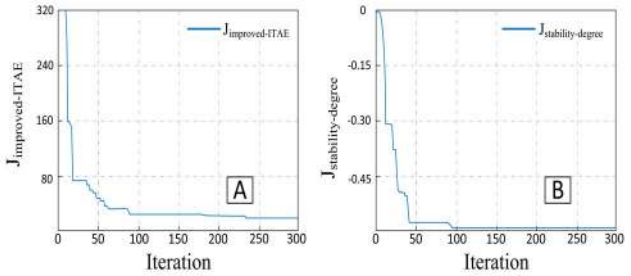

FIGURE 9. Comparisons of convergence curves for two schemes.

Thirdly, it is necessary for setting the weight coefficients w_1 and w_2 in improved-ITAE criteria to primarily take into account requirements for dynamic performance indicators in operation. Following this principle, they are set to $[w_1, w_2] = [0.9, 0.1]$ [20].

Fourthly, in order to avoid the randomness of PSO algorithm, 100 trials are tried and average results are obtained. For searching optimized PI parameters, the adopted searching ranges are the same as typical ones mentioned in Part B, Section III, stricted to $k_{p0} \in$ [0.5,20] and $k_{i0} \in$ [0.05,10] [20], [25].

Finally, optimization is carried out with MATLAB/SIMULINK, considering improved-ITAE rule and stability-degree criteria control schemes respectively. The convergence curves of objective function J are plotted in Figure 9.

The illustration from Figure 9 appears that the fitness function can converge in two cases respectively, and rates of two converges are close. When performing in proposed criteria, the searching area is smaller as result of the boundary requirement for stability with $\max(\sigma_i) < 0$.

In addition, the comparisons of function solutions and values are revealed in Table 2.

D. OPTIMIZATION PROCESS ANALYSIS [45]

In stability-degree control scheme, the optimal solution is found on the basis of developing the position of the real part of extreme right eigenvalue. And all unsolved ones at $G_k = 10$, 30, 50, 100 and 300 are listed below.

The eigenvalue trajectories in s plane is roughly plotted in Figure 10, where solved eigenvalues are presented by red stars while those with respect to k_{p0} and k_{i0} are revealed by blue triangles. After optimisation, the real part of extreme right eigenvalue, which was -0.1461 is changed to -0.5807. Hence, the stability degree is improved by choosing optimum values for governing parameters.

Similarly, eigenvalues at $G_k = 10$, 30, 50, 100 and 300 in improved-ITAE control are around demonstrated in Table 4, and its eigenvalue trajectories is shown in Figure 11, where

TABLE 2. The comparisons of function solutions and values.

	improved-ITAE criteria		
	k_{p0}	k_{i0}	J_{min}
Average	3.5696	0.5080	18.0244
Optimal	*3.7579*	*0.5000*	16.3084
	stability-degree criteria		
	k_{p0}	k_{i0}	J_{min}
Average	7.9203	2.2492	-0.4278
Optimal	*7.4462*	*2.0961*	-0.5807

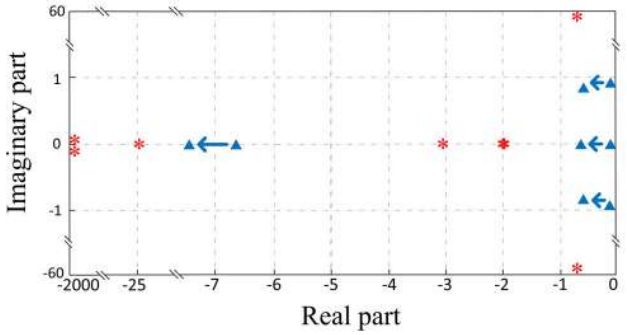

FIGURE 10. Eigenvalue trajectories under stability-degree rule.

TABLE 3. The optimization process under stability-degree rule.

G_k	10	30	50	100	300
k_{p0}	5.1401	8.5641	7.0801	7.3211	7.4462
k_{i0}	7.6620	2.3700	1.8634	1.8947	2.0961
J_{min}	-0.1461	-0.4499	-0.5571	-0.5616	-0.5807
eigenvalues with respect to k_{p0} *and* k_{i0}	-6.7184 -0.1461 ± 0.8811i -0.1516	-7.2250 -0.4734 ± 1.0115i -0.4499	-7.3403 -0.5571 ± 0.7262i -0.5655	-7.3861 -0.5616 ± 0.7900i -0.5712	-7.4048 -0.5862 ± 0.7994i -0.5807

TABLE 4. The optimization process under improved-ITAE rule.

G_k	10	30	50	100	300
k_{p0}	10.4701	5.5583	4.3258	3.6453	3.7579
k_{i0}	6.2530	3.0103	0.9889	0.5710	0.5000
J_{min}	644.9583	78.5620	43.0038	21.8371	16.3084
eigenvalues with respect to k_{p0} *and* k_{i0}	-7.8430 -0.0587 ± 1.1734i -1.0396	-7.4102 -0.1413 ± 0.6542i -1.7326	-7.3403 -0.1342 ± 0.3093i -1.7683	-6.6031 -0.2048 ± 0.1907i -1.8873	-6.6362 -0.2246 ± 0.1427i -1.9145

TABLE 5. Improvements on rotational speed and gate opening characteristics.

No.	Dynamic characteristics	Improved-ITAE criteria results	Sability-degree criteria results	Differences
1	Maximum speed deviation (pu)	0.0220	0.0150	0.32
2	Minimun speed deviation (pu)	-0.0214	-0.0149	0.30
3	Speed tuning time (s)	20	6	0.70
4	Maximum gate opening deviation (pu)	0.1244	0.1547	-0.24
5	Minimun gate opening deviation (pu)	-0.0291	-0.0592	-1.03
6	Gate opening tuning time (s)	20	6	0.70

where *difference* = ((*improved-ITAE criteria result*)–(*stability-degree criteria result*))/(*improved-ITAE criteria result*)

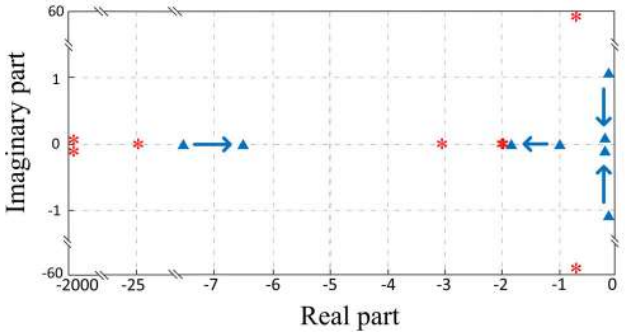

FIGURE 11. Eigenvalue trajectories under improved-ITAE rule.

solved eigenvalues are presented by red stars while those with respect to k_{p0} and k_{i0} are revealed by blue triangles. After improved-ITAE optimisation, the imaginary part of eigenvalue is changed from 1.1734 to 0.1427, which tends to minimize the system overshoot [16], [17].

V. DYNAMIC SIMULATION AND RESULTS

Indicial response of a 400MW on-grid ASPSU, performed in PSCAD/EMTDC, is aimed to vertify the improvement in transient performance of rotational speed and guide vane opening by optimal control parameters for speed governor of ASPSU based on stability-degree criteria proposed.

Model parameters used in simulation are given in Appendix B [26]. And the tunable operations follow those of the practical example in Ohkawachi power station reported, mentioned in details in Part E, Section II [1], [10].

The simulation results are illustrated in Figure 12. There are three diagrams of dynamic characteristics from top to bottom, i.e. power command and output, rotational speed, and guide vane opening. And with the same power command, transient speed and guide vane opening of ASPSU with stability-degree-criteria control strategy are shown by the solid blue outlines while those with improved-ITAE-criteria control method are revealed by the dashed yellow outlines.

From comparisons observed in Figure 12, power output can rapidly respond to power instruction within 0.2s in both improved-ITAE-criteria and stability-degree-criteria methods, with an inset zoomed view during active power change. On-grid ASPSU adopting stability-degree criteria control method has more desirable dynamic rotational speed and gate opening characteristics.

TABLE 6. Comparisons of stability-degree criteria simulated results and measurements.

No.	Dynamic characteristics	Sability-degree criteria results	Measurements
1	Maximum speed deviation (pu)	0.0150	0.0125
2	Minimun speed deviation (pu)	-0.0149	-0.0192
3	Speed tuning time (s)	6	24
4	Maximum gate opening deviation (pu)	0.1547	0.117
5	Minimun gate opening deviation (pu)	-0.0592	-0.061
6	Gate opening tuning time (s)	6	25

When in improved-ITAE-criteria method, beginning with t = 40s, rotational speed gradually touches the bottom with 0.0214pu deviation and after 20s, it reverts to steady state. At the same time, wicket gate reaches the maximum point with 0.1244pu deviation and after 20s, it stabilizes at a greater opening. Starting from t = 94s, runner speed progressively reaches the highest with 0.0220pu deviation and after 20s, it returns to steady state. Meanwhile, wicket gate reaches the minimum point with 0.0291pu deviation and after 20s, it stabilizes at a smaller opening.

When in stability-degree-criteria approach, starting from t = 40s, rotational speed hits rock bottom with 0.0149pu deviation and after 6s, it reverts to steady state. Simultaneously, wicket gate reaches the maximum point with 0.1547pu deviation and after 6s, it stabilizes at a larger opening. Beginning with t = 94s, runner speed peaks with 0.0150pu deviation and after 6s, it returns to steady state. Meanwhile, wicket gate reaches the minimum point with 0.0592pu deviation and after 6s, it stabilizes at a smaller opening.

Dynamic characteristics in two cases are listed in Table 5. In regard to runner speed, the tuning time significantly reduces by 0.7 and the deviation decreases by more than 0.3 in novel method. About guide vane opening, its tuning time also reduces by 0.7 while its deviation increases on different levels.

To figure out whether the simulated guide vane opening deviation results are accepted or not, stability-degree criteria simulated results are compared to measurement data, shown in Table 6.

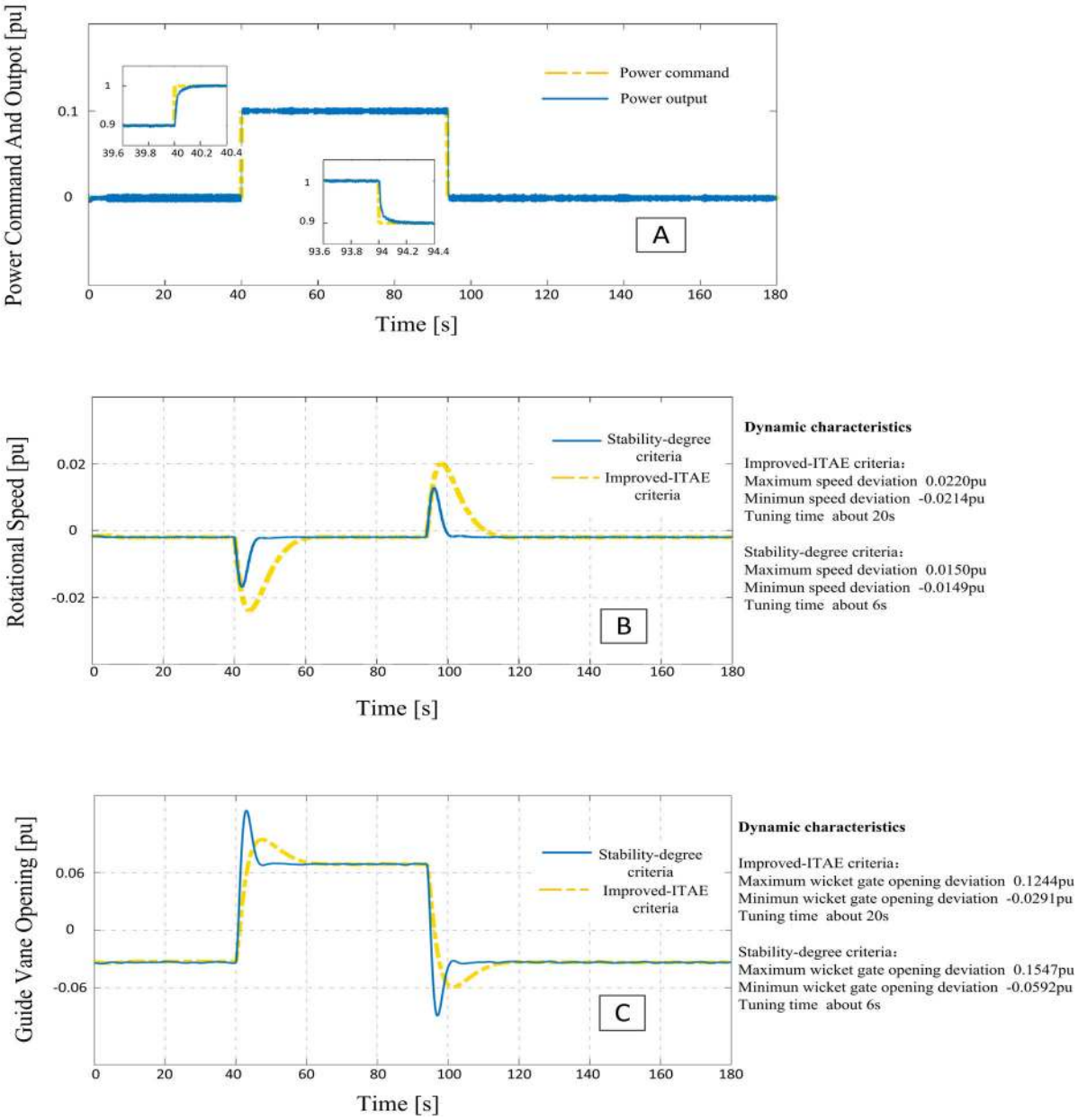

FIGURE 12. Comparisons in dynamic characteristics of ASPSU under stability-degree-criteria control strategy and improved-ITAE-criteria control method: (A) power command and output, (B) rotational speed, (C) guide vane opening.

From Table 4, minimum gate opening deviation simulation result is close to the measurement, with 0.03 difference while maximum gate opening deviation simulation result is worse than that of records, with 0.3 difference. It is possible that the plant operating in practice adopts a direct control method of vane opening [10].

VI. CONCLUSION

Superior transient behavior of on-grid ASPSU in maintaining active power balance is realized by coordinated control between excitation system and speed governing system. Nevertheless, available literatures on dynamic behavior of ASPSU have focused on its excitation system, which is incomplete.

In this way, the current paper first shed the light upon improving the dynamic performance of on-grid ASPSU from the perspective of modifying speed regulator control method. There are three main contributions:

1) On the basis of the dynamic ASPSU model, the small-signal-stability model of ASPSU is first established;

2) Under the assumption of the small-signal-stability model, the influence of PI governor parameters on the stability degree which builds the bridge between eigenvalues and transient performance of ASPSU is analyzed;

3) Instead of improved-ITAE rule based on external expression indexes, a novel stability-degree criteria is presented to optimise the parameters for regulator of ASPSU.

When implementing the demonstrated control method, the indicial response of a 400MW on-grid ASPSU is developed in terms of dynamic tuning time of both speed and guide vane opening with a 0.7 reduction as well as maximum/minimum speed deviation leading to a 0.3 reduction.

In the end, this study could be extended in the following aspects: (1) instead of PI controller, more advanced controllers will be carried out to realize online optimal determination under different steady-state operations. (2) there are various operating conditions of on-grid ASPSU including pumping mode, so its transient performance under other conditions also need to be explored in depth.

APPENDIX A [1], [10]

Maximum system input = 400MW, Maximum system output = 320MW, Generator terminal voltage = 18kV, Rated cycloconverter capacity = 72MVA, Rated cycloconverter voltage = 5.2kV.

APPENDIX B [26]

Equivalent time constant of pilot valve and servo motor $T_a = 0.2$s, Water time constant $T_w = 0.5$s, Inertia constant $T_J = 11$s, Rate limit of guide vane opening = 0.1pu.s^{-1}, Resistance of the stator winding $R_s = 0.0115$pu, Resistance of the rotor winding $R_r = 0.0128$pu, Self-inductance of the stator winding $L_s = 1.3$pu, Self-inductance of the rotor winding $L_r = 1.3$pu, Mutual inductance $L_m = 3.475$pu.

REFERENCES

[1] T. Kuwabara, A. Shibuya, H. Furuta, E. Kita, and K. Mitsuhashi, "Design and dynamic response characteristics of 400 MW adjustable speed pumped storage unit for Ohkawachi power station," *IEEE Trans. Energy Convers.*, vol. 11, no. 2, pp. 376–384, Jun. 1996.

[2] N. Sivakumar, D. Das, and N. P. Padhy, "Variable speed operation of reversible pump-turbines at Kadamparai pumped storage plant—A case study," *Energy Convers. Manage.*, vol. 78, pp. 96–104, Feb. 2014.

[3] M. Valavi and A. Nysveen, "Variable-speed operation of hydropower plants: A look at the past, present, and future," *IEEE Ind. Appl. Mag.*, vol. 24, no. 5, pp. 18–27, Sep. 2018.

[4] E. Muljadi, M. Singh, V. Gevorgian, M. Mohanpurkar, R. Hovsapian, and V. Koritarov, "Dynamic modeling of adjustable-speed pumped storage hydropower plant," in *Proc. IEEE Power Energy Soc. Gen. Meeting*, Denver, CO, USA, Jul. 2015, pp. 1–5.

[5] X. Shi, Y. Shi, W. Yan, G. Zhong, C. Yi, and X. Niu, "Analysis of operation characteristics of adjustable-speed pumped storage hydropower unit with AC excitation," in *Proc. IEEE 3rd Int. Electr. Energy Conf. (CIEEC)*, Beijing, China, Sep. 2019, pp. 862–868.

[6] L. Belhadji, S. Bacha, I. Munteanu, and D. Roye, "Control of a small variable speed pumped-storage power plant," in *Proc. 4th Int. Conf. Power Eng., Energy Electr. Drives*, Istanbul, Turkey, May 2013, pp. 787–792.

[7] A. Bocquel and J. Janning, "Analysis of a 300 MW variable speed drive for pump-storage plant applications," in *Proc. Eur. Conf. Power Electron. Appl.*, Dresden, Germany, Sep. 2005, p. 10.

[8] F. Wang and J. Jiang, "A novel static frequency converter based on multilevel cascaded H-bridge used for the startup of synchronous motor in pumped-storage power station," *Energy Convers. Manage.*, vol. 52, no. 5, pp. 2085–2091, May 2011.

[9] A. Joseph and T. R. Chelliah, "A review of power electronic converters for variable speed pumped storage plants: Configurations, operational challenges, and future scopes," *IEEE J. Emerg. Sel. Topics Power Electron.*, vol. 6, no. 1, pp. 103–119, Mar. 2018.

[10] J.-K. Lung, Y. Lu, W.-L. Hung, and W.-S. Kao, "Modeling and dynamic simulations of doubly fed adjustable-speed pumped storage units," *IEEE Trans. Energy Convers.*, vol. 22, no. 2, pp. 250–258, Jun. 2007.

[11] L. Ji, J. Sun, M. Zhou, and W. Tian, "AC excitation control strategy of variable speed pumped storage units based on active disturbance rejection control," *J. Eng.*, vol. 2017, no. 13, pp. 1195–1199, Jan. 2017.

[12] W. Hu, P. Zhang, Z. Chen, J. Li, S. Chen, and W. Ruan, "Model-based control for doubly fed adjustable-speed pumped storage units with fast power support," in *Proc. 13th IEEE Conf. Ind. Electron. Appl. (ICIEA)*, Wuhan, China, May 2018, pp. 2227–2232.

[13] J. Feltes, Y. Kazachkov, and B. Gong, "Modeling adjustable speed pumped storage hydro units employing doubly-fed induction machines," Argonne Nat. Lab., Lemont, IL, USA, Tech. Rep. ANL/DIS-13/06, 2013.

[14] V. Koritarov, T. Veselka, J. Gasper, B. Bethke, A. Botterud, J. H. Wang, M. Mahalik, Z. Zhou, and C. Milostan, "Modeling and analysis of value of advanced pumped storage hydropower in the United States," Argonne Nat. Lab., Lemont, IL, USA, Tech. Rep. ANL/DIS-14/07, 2014.

[15] A. O'Dwyer, *Handbook of PI and PID Controller Tuning Rules*. London, U.K.: Imperial College Press, 2003.

[16] D. Graham and C. R. Lathrop, "The influence of time scale and gain on criteria for servomechanism performance," *Trans. Amer. Inst. Electr. Eng., II, Appl. Ind.*, vol. 73, no. 3, pp. 153–158, Jul. 1954.

[17] H. Panagopoulos, T. Hägglund, and K. J. Åström, "Design of PID controllers based on constrained optimisation," *IEE Proc.-Control Theory Appl.*, vol. 149, no. 1, pp. 32–40, Jan. 2002.

[18] A. K. Barik and D. C. Das, "Active power management of isolated renewable microgrid generating power from rooftop solar arrays, sewage waters and solid urban wastes of a smart city using salp swarm algorithm," in *Proc. Technol. Smart-City Energy Secur. Power (ICSESP)*, Bhubaneswar, India, Mar. 2018, pp. 1–6.

[19] B. Mohanty, S. Panda, and P. K. Hota, "Controller parameters tuning of differential evolution algorithm and its application to load frequency control of multi-source power system," *Int. J. Electr. Power Energy Syst.*, vol. 54, pp. 77–85, Jan. 2014.

[20] Y. Xu, J. Zhou, X. Xue, W. Fu, W. Zhu, and C. Li, "An adaptively fast fuzzy fractional order PID control for pumped storage hydro unit using improved gravitational search algorithm," *Energy Convers. Manage.*, vol. 111, pp. 67–78, Mar. 2016.

[21] P. Kundur, *Power System Stability and Control*. New York, NY, USA: McGraw-Hill, 1994.

[22] C. Trivedi, E. Agnalt, and O. G. Dahlhaug, "Investigations of unsteady pressure loading in a francis turbine during variable-speed operation," *Renew. Energy*, vol. 113, pp. 397–410, Dec. 2017.

[23] Y. Pannatier, C. Nicolet, B. Kawkabani, J. L. Deniau, A. Schwery, F. Avellan, and J. J. Simond, "Transient behavior of variable speed pump-turbine units," in *Proc. 24th IAHR Symp. Hydraulic Machinery Syst.*, Foz do Iguaçu, Brazil, Jan. 2008, pp. 1–14.

[24] M. H. Chaudhry, *Applied Hydraulic Transients*, 3rd ed. New York, NY, USA: Van Nostrand, 2014.

[25] G. Zhao and J. Ren, "Research on an output power model of a doubly-fed variable-speed pumped storage unit with switching process," *Appl. Sci.*, vol. 9, no. 16, p. 3368, Aug. 2019.

[26] W. Yang and J. Yang, "Advantage of variable-speed pumped storage plants for mitigating wind power variations: Integrated modelling and performance assessment," *Appl. Energy*, vol. 237, pp. 720–732, Mar. 2019.

[27] C. Feng, C. Li, L. Chang, T. Ding, and Z. Mai, "Advantage analysis of variable-speed pumped storage units in renewable energy power grid: Mechanism of avoiding S-shaped region," *Int. J. Electr. Power Energy Syst.*, vol. 120, Sep. 2020, Art. no. 105976.

[28] R. Quan and W. Pan, "A low-order system frequency response model for DFIG distributed wind power generation systems based on small signal analysis," *Energies*, vol. 10, no. 5, p. 657, May 2017.

[29] P. S. Subudhi and S. Krithiga, "PV and grid interfaced plug-in EV battery charger operating in P-VG, P-V and V-G modes," *Int. J. Recent Technol. Eng.*, vol. 8, no. 2, pp. 3431–3443, Jul. 2019.

[30] P. S. Subudhi, K. Subramanian, and B. B. J. D. Retnam, "Wireless electric vehicle battery-charging system for solar-powered residential applications," *Int. J. Power Energy Syst.*, vol. 39, no. 3, pp. 130–140, 2019.

[31] J. Lin, G. J. Li, Y. Z. Sun, and X. Li, "Small-signal analysis and control system parameter optimization for DFIG wind turbines," (in Chinese), *Autom. Electr. Power Syst.*, vol. 33, no. 5, pp. 86–90, 2009.
[32] L. Yang, G. Y. Yang, Z. Xu, Z. Y. Dong, K. P. Wong, and X. Ma, "Optimal controller design of a doubly-fed induction generator wind turbine system for small signal stability enhancement," *IET Gener., Transmiss. Distribution*, vol. 4, no. 5, p. 579, 2010.
[33] B. Dong, S. Asgarpoor, and W. Qiao, "ANN-based adaptive PI control for wind turbine with doubly fed induction generator," in *Proc. North Amer. Power Symp.*, Boston, MA, USA, Aug. 2011, pp. 1–6.
[34] G. Bitew, M. Han, S. Mekonnen, and P. Simiyu, "A variable speed pumped storage system based on droop-fed vector control strategy for grid frequency and AC-bus voltage stability," *Electronics*, vol. 7, no. 7, p. 108, Jul. 2018.
[35] F. Wu, X. P. Zhang, K. Godfrey, and P. Ju, "Small signal stability analysis and optimal control of a wind turbine with doubly fed induction generator," *IET Gener., Transmiss. Distrib.*, vol. 1, no. 5, pp. 751–760, Sep. 2007.
[36] S. J. Han, "Robust and optimal PID controller synthesis for linear time invariant systems," Ph.D. dissertation, Dept. Elect. Eng., Texas A&M Univ., College Station, TX, USA, 2019.
[37] I. Fiodorov, B. Izvoreanu, and I. Cojuhari, "Synthesis of robust PID controller by the maximum stability degree criterion," in *Proc. 20th Int. Conf. Control Syst. Comput. Sci.*, Bucharest, Romania, May 2015, pp. 57–64.
[38] J. Kennedy and R. Eberhart, "Particle swarm optimization," in *Proc. IEEE Int. Conf. Neural Netw.*, Perth, WA, Australia, Nov. 1995, pp. 1942–1948.
[39] Y. Shi and R. Eberhart, "A modified particle swarm optimizer," in *Proc. IEEE Int. Conf. Evol. Comput. IEEE World Congr. Comput. Intell.*, Anchorage, AK, USA, May 1998, pp. 69–73.
[40] R.-J. Wai, J.-D. Lee, and K.-L. Chuang, "Real-time PID control strategy for maglev transportation system via particle swarm optimization," *IEEE Trans. Ind. Electron.*, vol. 58, no. 2, pp. 629–646, Feb. 2011.
[41] A. N. Abdalla, K. Li, S. J. Cheng, J. Y. Wen, and J. Zhang, "Parameter identification of governor-turbine system based on a PSO algorithm," in *Proc. 1st Int. Conf. Bio-Inspired Comput.*, Wuhan, China, Sep. 2006, pp. 1–6.
[42] Y. Shi, "Optimization of PID parameters of hydroelectric generator based on adaptive inertia weight PSO," in *Proc. IEEE 8th Joint Int. Inf. Technol. Artif. Intell. Conf. (ITAIC)*, Chongqing, China, May 2019, pp. 1854–1857.
[43] H. Kawajiri, Y. Enomoto, and S. Kurosawa, "Design optimization method for Francis turbine," in *Proc. 27th IAHR Symp. Hydraulic Machinery Syst.*, Montreal, QC, Canada, Sep. 2014.
[44] H. Fang, L. Chen, and Z. Shen, "Application of an improved PSO algorithm to optimal tuning of PID gains for water turbine governor," *Energy Convers. Manage.*, vol. 52, no. 4, pp. 1763–1770, Apr. 2011.
[45] M. Clerc and J. Kennedy, "The particle swarm–explosion, stability, and convergence in a multidimensional complex space," *IEEE Trans. Evol. Comput.*, vol. 6, no. 1, pp. 58–73, Feb. 2002.

WENXIA PAN received the B.S. and M.S. degrees from Wuhan University, Wuhan, China, in 1982 and 1987, respectively, and the Ph.D. degree from Hohai University, Nanjing, China, in 2004. She is currently a Professor of electrical engineering with Hohai University. She has published two research books. She has authored or coauthored more than 100 journal articles. Her current research interests include renewable energy generation systems and high-voltage and insulation technology.

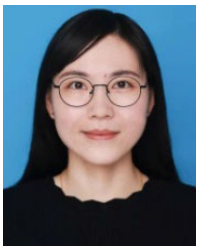

ZHU ZHU received the B.S. degree in electrical engineering from the North China University of Water Resources and Electric Power, Zhengzhou, China, in 2010, and the M.S. degree in photovoltaic and renewable energy engineering from the University of New South Wales (UNSW), Sydney, Australia, in 2011. She is currently pursuing the Ph.D. degree in electrical engineering with Hohai University, Nanjing, China. Her main research interest includes renewable energy generation technology.

TONGCHUI LIU received the B.S. degree from Xuchang University and the M.S. degree from Hohai University, Nanjing, China, in 2012 and 2015, respectively, where he is currently pursuing the Ph.D. degree in electrical engineering. He is also an Engineer with State Grid Ningbo Power Supply Company, Ningbo, China. His main research interest includes renewable energy generation technology.

MINGYANG LIU (Member, IEEE) received the B.S. degree in electrical engineering from the North China University of Water Resources and Electric Power, Zhengzhou, China, in 2013, and the Ph.D. degree in electrical engineering from Hohai University, Nanjing, China, in 2019. He is currently an Electrical Engineer with State Grid Henan Electric Power Research Institute, Zhengzhou. His research interests include power systems analysis and wind power generation.

WEI TIAN received the B.S. and M.S. degrees from Wuhan University, Wuhan, China, in 2000 and 2005, respectively. He is currently pursuing the Ph.D. degree in electrical engineering with Hohai University, Nanjing, China. He is also a Senior Engineer with NARI Technology Company Ltd. His main research interest includes renewable energy generation technology.